Overview of High-density FRC Research on FRX-L at Los Alamos National Laboratory

J.M. Taccetti, T.P. Intrator, S.Y. Zhang, G.A. Wurden, R.J. Maqueda, M.Tuszewski, R. Siemon, D. Begay, E. Mignardot, P. Sanchez, B. Waganaar, R. Aragonez, *Los Alamos National Laboratory, Los Alamos, NM 87545 USA*

C. Grabowski, E. Ruden, J.H. Degnan, W. Sommars *Air Force Research Laboratory, Albuquerque, NM USA*

Abstract

We present an overview of the FRC research on the Field Reversed configuration eXperiment – Liner (FRX-L) device at Los Alamos National Laboratory. This is a target plasma 'injector' to be used for magnetized target fusion (MTF) applications. MTF is an approach to fusion wherein a magnetized target plasma is compressed to fusion conditions. Our target plasma is an FRC because it has the required closed-field-line topology, and is translatable and compressible. The existing empirical database also indicates that the type of FRC required for MTF would be achievable. FRX-L includes the formation and translation of the FRC into a mock target chamber. We are currently in the process of forming the high-density FRC.

Introduction

The two more conventional paths to fusion lie at the two extremes of the spectrum with respect to plasma lifetime and density. Magnetic fusion energy, or MFE as it is commonly referred to, deals with long times (milliseconds to seconds) and low initial densities (~10^{14} cm^{-3}). In this case, a magnetic field is used to contain a plasma configuration for long periods of time. Some examples of this method are the tokamak, the FRC, and the spheromak. The advantages of this path to fusion include the possibility of a low but constant energy source. The principal disadvantage of this method is the inherent difficulty of trying to contain the plasma for a long time. At the other extreme of the spectrum lies inertial confinement fusion, or ICF. This method proposes obtaining fusion in short times but at high density, resulting in short pulses of high energy. A solid pellet of fusion fuel is heated on its outer surface, and the expelled gases cause the outer shell to compress the inner fuel. ICF has the advantage that one does not need to bother with magnetic fields. In addition, high density means higher fusion reactivity. But this comes at a price. At these densities one requires extremely high uniformity, not only in engineering of the pellet but also in the delivery of the heating to the pellet due to the high volume compression ratios required [1].

Magnetized Target Fusion, or MTF for short, combines the advantages of these two methods [1-3]. A target plasma is compressed, as in ICF, but this target is preheated and has magnetic fields embedded in it to insulate the plasma from the wall. Compared to ICF, this relaxes the requirements on compression uniformity and velocity. MTF can be separated into three steps: formation of target plasma, translation of target plasma into target chamber (cylindrical liner, or 'can'), and compression of the chamber along with the plasma to fusion conditions, coupling the compressional energy into the plasma (see Fig. 1). The requirements for the target are a starting temperature of $T_e \sim T_i \sim$50-300 eV, a density of 10^{17} to 10^{18} cm^{-3}, and a closed field line topology with a magnetic field of ~5 T. The compression is achieved by driving a large current down the axis of the liner, thereby causing it to pinch, though maintaining its shape at least until the required compression factor is reached (10× for our

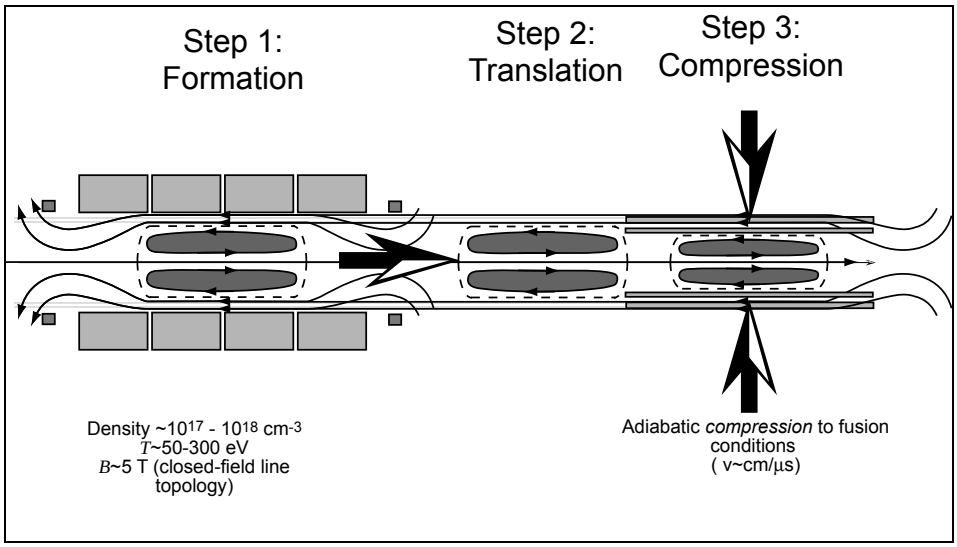

Fig. 1. The three steps of MTF.

case). This compression is adiabatic, with speeds on the order of cm/μs, which are easily achievable with existing pulsed-power facilities, such as the Atlas facility at LANL [4,5].

Fusion reactivity is given by the formula

$$R = n_D n_T \left\langle \sigma_{DT} v \right\rangle = \frac{1}{4} n^2 \left\langle \sigma_{DT} v \right\rangle, \tag{1}$$

where n_D and n_T are densities of deuterium and tritium, $\langle\sigma_{DT}v\rangle$ is the average cross-section for a DT reaction, and we are assuming $n_D = n_T = n/2$ [6]. As stated before, higher density improves the reaction rate by many orders of magnitude over conventional MFE. All characteristic plasma scale lengths also decrease with increasing plasma density, thereby decreasing system size with respect to MFE. At the same time, magnetic insulation greatly reduces the power and precision required to compressionally heat the plasma to fusion conditions.

We chose to use the FRC as the target plasma. FRCs have the required closed-field-line topology, and are translatable and compressible. The existing empirical database also indicates that the type of FRC required for MTF would be achievable [7]. Los Alamos National Laboratory and Air Force Research Laboratory in Albuquerque are currently collaborating on developing a target FRC with the characteristics outlined above. FRX-L, for field-reversed configuration experiment – liner, includes the formation and translation of the FRC into a mock target chamber. We are currently in the process of forming the high-density FRC.

FRX-L experimental design

The principal components of the FRX-L plasma device are shown in Fig. 2 below. FRX-L consists basically of a theta-pinch coil (the theta coil is a straight coil, *i.e.* it has no mirror fields at the ends) driven by various capacitor banks in parallel, precisely timed to form, contain, and translate an FRC with the temperature, density, and lifetime appropriate for MTF. There are a total of four capacitor banks used for this purpose: main, pre-ionization (PI), bias, and cusp/mirror banks.

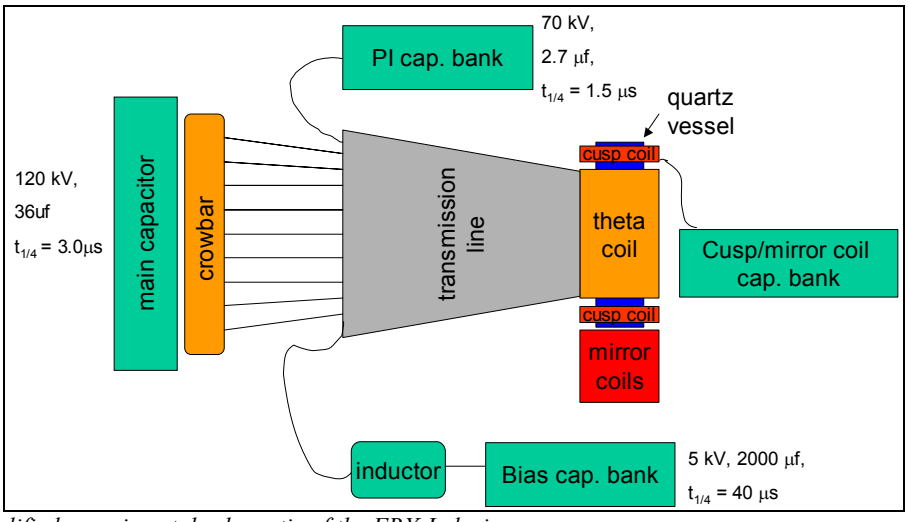

Fig. 2. Simplified experimental schematic of the FRX-L device.

The bias bank produces the low-level slowly-varying (as close to DC as possible desired during plasma lifetime) magnetic field which later becomes trapped to form the FRC. This is a 2000 μf, 10kV bank, with a quarter cycle time, $t_{1/4}$, equal to 40 μs. When the bias bank discharge is initiated, a static fill of D_2 gas (p_0=20-40 mTorr) is present in the chamber, a 0.5 mm thick walled quartz discharge tube inside of the theta coil. Upon reaching the first peak of the bias field, the PI bank is triggered. This is a 70 kV, 2.7 μf, $t_{1/4}$ = 1.5 μs bank used to ionize the gas by ringing the magnetic field at high frequency (usually known as the θ-PI method). We chose this pre-ionization from among the various possibilities [7] due to its simplicity – no additional hardware except for the bank is necessary on the experiment – and cleanliness – the only impurities possible are due to the quartz tube interacting with the plasma. Once a sufficiently high ionization level is reached, such that the bias field lines are properly frozen into the plasma, the main bank is triggered. This bank is connected such that the field is opposite in direction to the original bias field. It is also about 10 times larger in magnitude than the bias field (the bank is a 120 kV, 36 μf, $t_{1/4}$ = 3 μs). This causes the plasma to implode radially, due to $\boldsymbol{J}\times\boldsymbol{B}$ forces between the large induced azimuthal electric field and the frozen-in bias field. At some point, the fields reconnect near the ends of the coils, and field line tension then causes the plasma to compress axially.

The cusp/mirror coils consist of three pancake coils (10 turns each) in series, located at either end of the theta coil. These create a null in the bias field, and seed the reconnection to occur in the same place every time. The cusp field is also large enough that it makes a mirror magnetic field on top of the main bank field, thereby holding the FRC in place after formation. A 1 cm-thick stainless steel plate sits between each cusp coil and the theta-pinch coil to reduce mutual inductance between them. The bank driving the cusp coils consists of old FRX-C modules [8], 8000 μf total, 10 kV max voltage. It is made to also drive additional coils at one end of the cusp, forming a mirror field to 'catch' the FRC when it is translated out from the formation region. These must be slow enough to penetrate the thin (1 mm wall) aluminum liner.

Other important characteristics of the experiment are given in the table below, along with some design values.

Though we are currently making plasmas, the cusp/mirror coils have not been operated yet, and this presents problems with reproducibility. Without the cusps, the field null points occur outside of the theta coil, where field reconnection is more difficult due to decreased ionization levels. Reconnection is therefore most probably due to tearing of the field lines under the theta coil, making it very irreproducible. A simulation of the transient

Physical Constraints:	
Coil radius	r_c = 6.2 cm
Coil length	l_c = 36.0 cm
discharge tube radius	r_t = 5.25 cm
reversal electric field	E_θ = 0.15 (1.0*) kV/cm
fill pressure	p_0 = 20-40 mTorr
crowbar field	B_c = 1.5 T (5 T*)
Expected plasma parameters:	
separatrix radius	r_s ~ 3 cm
Plasma length	l_s = 30 cm

*Table 1. FRX-L experimental parameter (*denotes maximum operating values).*

axial magnetic field vs. axial distance from the midpoint of the coil is shown in Fig. 3. This simulation includes the steel plates at both ends of the theta coil but excludes the cusp fields. With the cusp coils operational, the field nulls will occur inside the theta coil, and the x-points should therefore easily form where these nulls occur. The cusp/mirror coils should be coming online this month.

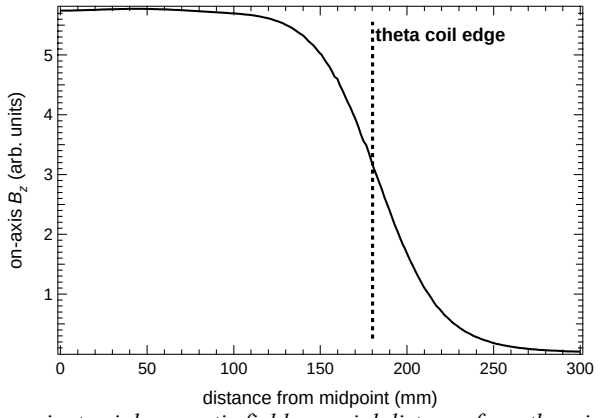

Fig. 3. Simulation of the transient axial magnetic field vs. axial distance from the midpoint of the coil (theta coil edge at 180 mm)

Diagnostics/Initial Results

The various diagnostics installed on FRX-L provide us with information on the different phases of the FRC formation sequence. A summary of the diagnostics along with the information they provide is given in Table 2 below. Due to space constraints, I will only describe a few of the diagnostics presented in this table and show results obtained with them.

The multi-chord He-Ne (633 nm) laser interferometer, designed by AFRL, has been recently modified to decrease interference drift with time. It is currently set up as a two-chord interferometer but will be upgraded to 8 chords. Abel inversion of the data will provide a density plot of a cross-section of the plasma as a function of time. At the moment the interferometer is set up at the midpoint of the theta coil, and the two chords are at r = 0, 2 cm. The line-average density traces vs. time for a particular shot where an FRC was formed are shown on Fig. 4. The pre-ionization period is labeled as θ-PI on the figure. After the θ-PI period, the reversal field is applied, and plasma lift-off occurs between 8 and 9 μs. The plasma continues to compress, but decompresses again after 10.3 μs, as the crowbarred field rings

Diagnostic	Information provided
flux loops & Bz probes	➢ separatrix radius, excluded field
H-beta line broadening	➢ density during PI stage
Multi-chord He-Ne red interferometer (side-on)	➢ density during formation
Multi-point Thomson scattering	➢ T_e, n
Optical tomography	➢ large-scale plasma behavior
Framing camera (end-on)	➢ large-scale plasma behavior
Bolometer	➢ radiated power
Multi-channel spectrometer	➢ Impurity line intensities vs time

Table 2. Summary of the installed diagnostics along with the information they provide.

down (more detail on this is provided below). As the field increases a second time and begins to compress, the density falls off suddenly. We believe this sudden disappearance of the FRC is due to uneven tearing reconnection at the ends of the FRC, probably causing some initial axial motion, which increases when the second compression is initiated. This axial motion is corroborated by flux exclusion measurements, as presented below.

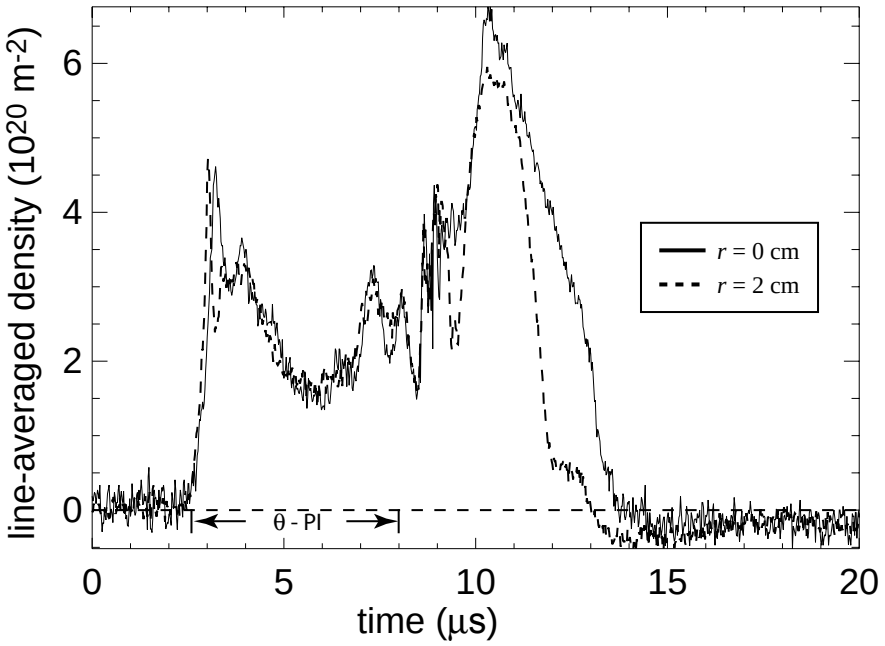

Fig. 4. Line-averaged density traces at midpoint of theta coil, r = 0 cm (solid) and r = 2 cm (dashed).

Magnetic field probes and flux loops fielded in the space between the discharge tube and the theta coil provide information on the FRC separatrix shape as a function of time [9]. The diamagnetic FRC excludes flux. As the total flux of the theta coil is conserved, but the area which it threads is decreased by the existence of the FRC, the magnetic field detected by the probes increases. Signals from a magnetic probe and flux loop pair are fed into an adding circuit. The flux loop polarity is reversed, such that the two signals are opposed. The resulting signal is zeroed out during a vacuum shot by attenuating one of the two inputs. During a gas discharge, the output signal will seem larger due to the increase in the magnetic field. This is a measure of the excluded flux. After further analysis, one obtains the signal shown in Fig. 5. This pertains to the same shot as Fig. 4. The noise threshold in Fig. 5 is on the order of 0.5 cm.

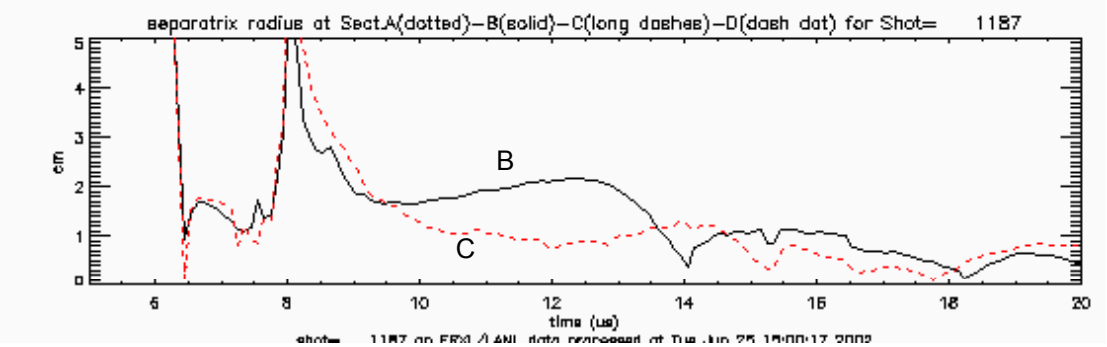

Fig. 5. Separatrix radius for two innermost segments of the theta coil. Solid – segment B, Dashed – segment C.

The FRX-L theta coil is split into four equal segments, labeled A to D, each 8.25 cm long, with a 1 cm gap between them. The plot shows the excluded flux radius (approximately the same as the separatrix radius, r_s) for segments B and C, the inner two segments of the coil. As shown before, field reversal commences at ~ 8 μs. After an initial expansion, we see the plasma 'lift-off' from the wall and the separatrix beginning to decrease. Segment B r_s decreases faster and is shocked, as seen by the small peak around 9 μs, while for C it does so more slowly and smoothly. The separatrix continues to decrease below segment C, while it grows below segment B. But at 13.5 μs, as the crowbarred field reaches a minimum, we note the plasma seems to shift from segment B to C, though it disappears promptly as the field increases once again. This behavior indicates reconnection is occurring in unexpected locations and asymmetrically, causing the plasma to have an axial velocity component during our shots without cusps coils, similar to what has been seen previously by others [10]. (Our present theta coil has no mirror fields, and therefore no way to curtail this axial motion, resulting in a sudden loss of the plasma.)

The magnetic probe design is limited by both by the high voltage environment in which it must operate and the and narrow gap inside of which it must fit (only 5 mm exists between the discharge tube and the theta coil, not counting the polyethylene insulation covering approximately half of the surface of the discharge tube).

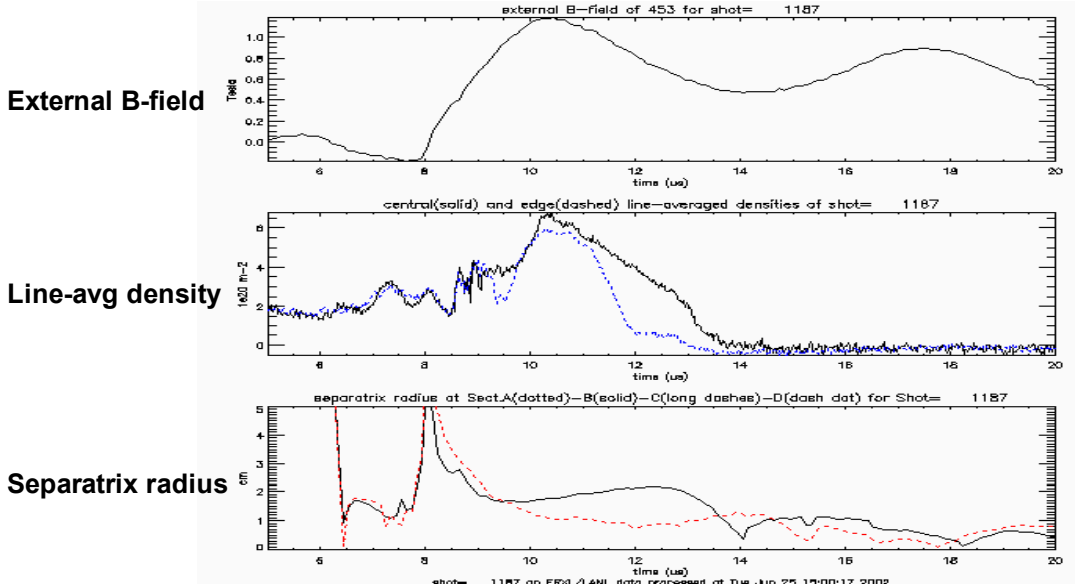

Fig. 6. Comparison of the external magnetic field with previously shown line-averaged density and separatrix radius (all for the same shot).

Figure 6 compares an external magnetic field probe, the line averaged density traces, and the separatrix radius for the same shot. This shows clearly how excluded flux and density both decrease as the crowbarred field rings down.

One of the most important diagnostics being installed is a Multi-point Thomson Scattering system. It consists of a 20 J pulsed ruby laser, the input and output ports through the experiment, and collecting optics. The laser traverses the theta coil region at an angle, such that it cuts through the high density regions of the FRC. The collecting optics, arrayed along the z-axis, are brought up close to the discharge tube by drilling holes in the theta coil. The detector views through the theta coil at six groups of 3 spatial points each, providing data at different axial and radial locations. The system is still in its testing phase, but we hope to have first data very soon.

Future Directions

The present crowbar design is not optimal. It is not well matched to the system and causes excessive modulation in the crowbarred *B*. The best crowbarred field is such that the first minimum following the peak reversed field is 41% of this peak field. As this containing field oscillates, the FRC increases and decreases in radius, running the risk of hitting the walls; it also stretches axially, possibly beyond the ends of the theta coil, into regions of cold un-ionized gas. Possible solutions for the crowbar ringing problem include reducing the inductance of the crowbar switch and operating at higher main bank voltages, resulting in better rail gap conduction (and possibly also lower inductance). Still, these are not easy solutions to implement. We will know how much of a real concern the ringing crowbar is after we fire with the cusp/mirror coils.

Our main capacitor bank is a Marx bank and utilizes rail-gap switches for operation. The previously installed rail-gap switch design was prone to self-breakdown and did not survive them very well. Due to recurring problems with this rail-gap switch, we have switched over to more robust Atlas-style gaps [11]. The improved contouring of the inside surfaces of the gaps should decrease the chance of flashovers which cause pre-fires and damage to gaps.

Summary

Magnetized target fusion is the method by which a magnetized target plasma of T~300 eV and n~10^{17}cm^{-3} is imploded to fusion conditions. High-density FRCs make ideal MTF targets, due to their closed field line configuration, and the possibility to translate and compress them. In addition, the existing empirical database suggests it is possible to form FRCs of the required temperature, density, and lifetime.

We still have several obstacles to overcome, including the addition of the cusp fields and the reduction of the crowbar ringing. The absence of the cusps is believed to be the primary cause for the low reproducibility of the FRC formation. We are presently bringing the cusp banks online, and we hope to soon be forming more reproducible FRC plasmas and afterwards translating them into a surrogate aluminum liner.

Acknowledgments

This work was supported by DOE-OFES contract W-7405-ENG-36. This article is also listed as Los Alamos National Laboratory Report number LA-UR-02-6305.

References

1. R.E. Siemon, I.R. Lindemuth, and K.F. Schoenberg, Comments Plasma Phys. Controlled Fusion **18**, 363 (1999).
2. I.R. Lindemuth, R.E. Reinovsky, R.E. Chrien *et al.*, Phys. Rev. Lett.**75**, 1953 (1995).
3. R.C. Kirkpatrick, I.R. Lindemuth, M.S. Ward, Fusion Technology **27**, 201 (1995).
4. J.M. Taccetti, T.P. Intrator, F.J. Wysocki, *et al.*, Fusion Science and Technology **41**, 13 (2002).
5. T.P. Intrator, J.M. Taccetti, D.A. Clark, *et al.*, Nuclear Fusion **42**, 211 (2002).
6. S. Glasstone and R.H. Lovberg, Controlled Thermonuclear Reactions, (D. Van Nostrand, Princeton, 1960), p 11.
7. M. Tuszewski, Nucl. Fusion **28**, 2033 (1988).
8. R.E. Siemon, W.T. Armstrong, D.C. Barnes *et al.*, Fusion Technology **9**, 13 (1986).
9. M. Tuszewski, Phys. Fluids **24**, 2126 (1981).
10. A. Eberhagen and W. Grossmann, Z. Phys. **248**, 130 (1971).
11. W.M. Parsons, E.O. Ballard, R.R. Bartsch *et al.*, Los Alamos National Laboratory Report LA-UR-96-3440, 1997.